By Ricardo F. Aroca and Daniel J. Ross
Materials and Surface Science Group
University of Windsor, Windsor, Ontario, N9B 3P4, Canada
and
Concepción Domingo
Instituto de Estructura de la Materia, CSIC
Serrano, 123, 28006 Madrid, Spain

Surface-Enhanced Infrared Spectroscopy

INTRODUCTION

The discovery of surface-enhanced Raman scattering (SERS)[1–3] opened the field of surface-enhanced spectroscopy, including linear and nonlinear optical phenomena.[4,5] In particular, the realization of surface-enhanced infrared absorption (SEIRA)[6] permitted one to speak of a unified field of surface-enhanced vibrational spectroscopy (SEVS), supported by the enhanced Raman and infrared techniques. Since the enhancement factor in the absorption seems insignificant when compared with those of SERS, the SEIRA effect has not received the attention of SERS. The initial sporadic activity on the subject of SEIRA was largely concentrated in Japan and a look at the early work can be found in Osawa's review.[7] In the 1990s SEIRA received its share of attention, and there were several reports for both the practical and theoretical aspects of the phenomena.[8–11] Since the bulk of SEIRA work is recent, it is still of interest to demonstrate the effect itself, in particular the SEIRA spectra that can be obtained for the same system on different enhancing surfaces. The effect has been observed on island films of the coinage metals and a few other surfaces, most notably Pt,[11] Sn,[12] Pd, and Ru.[13,14] Recently, infrared enhanced absorption was demonstrated for anthracene coating polar dielectric nanoparticles of silicon carbide and aluminum oxide with a 100-fold enhancement.[15] In the latter experiments, SEIRA is explained as being the result of the enhanced optical fields at the surface of the particles when illuminated at the surface phonon resonance frequencies. It is pointed out that this phonon resonance effect is analogous to the plasmon resonance that is the basis for surface-enhanced Raman scattering and SEIRA in metals. The role of surface plasmons has been well documented and there is abundant literature on the subject. A review of the plasmon literature directly related to SEIRA and SERS is available.[16] Recently, the first study was reported on metal films with architectures designed to produce surface plasmons in the infrared region, permitting a comparison of SEIRA results for these films and those where plasmons are not detected.[17] The authors observed SEIRA in the region of a surface plasmon using engineered surfaces. When these results were compared to SEIRA on evaporated metal films, equivalent results were obtained.

The experiments have always been tailored to attain enhanced optical fields and thereby the explanation is given in terms of electromagnetic (EM) models. In his broad review on SEIRA, Osawa[7] discusses these models, which can quantitatively explain the effect, and the applications to the study of, electrochemical reactions. Following, and by analogy with, the interpretation accepted for SERS, it has been suggested that electromagnetic and chemical contributions are responsible for the observed infrared enhancement. The analogy cannot be stretched too far, since the so-called chemical contributions to SERS include additional multiplicative effects, such as charge transfer, that lead to resonance Raman scattering.[18,19] Computations of the EM enhancement using effective medium theories have been reviewed[20] and there is no question that there is a key contribution from enhanced local fields to SEIRA. There is an increase in the rate of absorption per unit volume that is proportional to

the energy density of the field at the appropriate frequency. The enhanced local field augments this energy density at the surface of particles where the adsorbed molecule resides. This local field varies according to several factors, size, shape, and the dielectric function, among others.[21] The enhancement varies from point to point and the average value is expected to match the observations. There are further consequences for the observed infrared spectrum from molecules adsorbed at these local fields. The local field may be highly polarized. Moskovits[4] has illustrated the implications of having a perpendicular polarized field, or a tangentially polarized field, in determining the surface selection rules. The latter is discussed separately using a physisorbed molecule as a study case. In addition, the local field changes the dipole moment of the adsorbed molecule (that one can call chemical effect) in a fashion similar to what is seen in electrochemistry,[22] producing a variation in the dipole moment derivatives and hence in the infrared intensity.

Griffiths et al.[11] reported a peculiar property in the symmetry of the SEIRA band shape of the CO on platinum. The band asymmetry has been studied in Griffiths' group and has been observed on Ag and Au island films. The effect can be simulated using the dielectric function of the metal and the substrate. However, the ''Fano band'' shape has attracted attention due possibly to a link of the observations with the dynamic interaction of the adsorbate vibrations with electron–hole pair excitations.[23] Expressions for an isolated vibrational mode, for a molecule adsorbed on a metallic surface, in the presence of electron–hole damping producing asymmetric line shape, have been derived by Langreth.[24]

The enhancement factors found in SEIRA can range up to 10^3, but are usually found to be in the 10–100 region at best. Compared to the very large enhancements observed in SERS, up to 10^{12}, this effect is not nearly as dramatic, and has attracted less interest. However, even this small enhancement can be used to detect monolayers of films.[9] Although SEIRA does not yield the enhancement necessary for single-molecule detection as SERS does,[25,26] SEIRA is a viable means of enhancing the infrared signal from adsorbed molecules on a variety of metals, semimetals, semiconductors, and polar dielectric nanostructures.

The present report is divided into four sections. The first part deals with the SEIRA experiments, involving transmission and reflection geometries. Secondly, theoretical models proposed to explain the electromagnetic SEIRA effect are examined, followed by a study case that illustrates the spectral interpretation and surface selection rules. Finally, a brief review of analytical applications is given.

THE EXPERIMENT

Preparation of Surface-Enhanced Infrared Absorption Substrates. Enhancement by SEIRA depends on the size, shape, and particle density of the selected metal island films. In the most widely used metal-underlayer configuration (sample–metal–substrate), film morphology is influenced by surface structure of the supporting substrate, as well as by the experimental conditions used during the film fabrication (for instance, evaporation rate and temperature of the supporting substrate). The supporting substrates commonly used include IR transparent materials (Si, Ge, CaF_2, BaF_2, KBr, ZnSe, ZnS, KRS-5, sapphire, MgO) and nontransparent materials such as glass, glassy carbon, polymers, and metals. The materials of the first group allow for transmission and/or reflection spectra, while the others are only adequate for external reflection measurements. Notably, low reflective materials could be optically favorable due to a reduced distortion of the band shape in the corresponding SEIRA spectrum. Metal-overlayer (metal–sample) and even sandwich (metal–sample–metal)[27] configurations have also been used successfully.

The SEIRA-active metal islands are commonly prepared by high vacuum evaporation of the metal onto a supporting substrate.[28] The typical system includes a stainless-steel chamber, a glass bell jar, a tungsten basket for placing the metal, a quartz crystal microbalance (QCM) for monitoring the film thickness, and the required vacuum pumps. Low melting point metals are evaporated by resistive thermal heating of the tungsten boat, while direct resistive heating of metal wires is used for metals with high melting point. Alloys can be prepared through simultaneous evaporation of both metals. Deposition rate of the metal is a crucial parameter for the shape and size of the islands, with slow rates (0.1–0.5 nm/min) generally giving the best enhancement. Optimal film thickness for maximum enhancement depends on the deposition rate; in fact, the optimization of both parameters must be made for each metal–substrate system. In an effort to control the morphology of the evaporated film and, therefore, its corresponding surface plasmon region, templates such as periodic particle array (PPA) films prepared by nanosphere lithography (NSL) have been employed.[17] Anodized porous Al surfaces and island films of different metals have been used as templates for subsequent metal evaporation.

The equipment for metal vacuum evaporation is routinely used in surface laboratories; however, it is not readily available in most IR laboratories. An alternative, and less expensive, method to form metal islands for SEIRA is electrochemical deposition, in which a suitable potential or current is applied to electrolyte solutions of salts of the metal to be deposited, either under potentiostatic, galvanostatic, or potential cycling conditions. The surface roughness, or island size, may be controlled by changing the concentration of the solution, the voltage or current applied, and the time utilized in the deposition. In some cases additives are used to control the morphology. The thickness of the film can be estimated from the charge passed during the deposition. In this

method the substrate on which the metal is to be deposited must have high electrical conductivity. For this reason materials such as glassy carbon or bulk metal have usually been used, although metal electrodeposition on Au-coated glass and n-type Si has also been reported. Electrochemical deposition has mainly been employed to prepare rough electrodes used in spectroelectrochemical studies, but its use has been proposed for manufacturing large amounts of recyclable SEIRA surfaces efficiently and at low cost.[29] The electrochemical preparation of gold particles and rods in anodic alumina templates have also been reported.[30]

Metal colloids can be employed as SEIRA-active nanostructures. They are prepared by reduction of metal ions. While aqueous metal colloids are one of the most common media employed in SERS due to the very low Raman scattering cross-sections of water, the extremely high IR absorption of water prevents their straightforward application in infrared measurements. Nevertheless, SEIRA enhancement using silver and gold colloidal particles has been reported. For instance, once the aqueous silver colloid is prepared, one aliquot amount (around 500 μL) is cast onto a KRS-5 substrate and is dried out. The process is repeated to obtain thick aggregated colloidal films.[31] On the other hand, colloidal gold bioconjugates (gold–protein complexes) have proved to be useful in immunoassays based on the SEIRA effect, either as wet samples collected by filtration on a porous polyethylene membrane, or as dry films.[32] Another possibility of using colloidal particles as SEIRA-active surfaces is to immobilize them on silane-derivatized glass substrates. We have succeeded in obtaining external reflection SEIRA spectra of 1,5-dimethylcytosine (1,5-DMC)[33] using, as active surfaces, laser-ablated silver colloids that were immobilized in an AMPTS (3-aminopropyltrimethoxysilane)-derivatized glass slide according to the method previously reported for SERS-active surfaces.[34] The SEIRA spectra of 1,5-DMC on ''evaporated'' and ''immobilized'' colloidal Ag nanoparticles are equivalent.

Metal sputtering (magnetron, diode) has also been used for deposition of nanoparticles of Ag,[10] Au,[35] and Pt[36] for SEIRA experiments.

Recently, the chemical (or electroless) deposition technique, in which the substrate is immersed in adequate metal plating solutions, has been applied successfully in preparing nanoparticle films of Au,[37] Ag,[38,39] Pt,[40] and Cu.[41] Atomic force microscopy (AFM) images of the chemically deposited Au films revealed an island structure similar to that of the vacuum evaporated Au films, with larger average dimensions of the islands (300 nm instead of 70 nm). The chemical deposition technique seems to be simple and cost effective, with good SEIRA enhancement. The technique also provides better adhesion of the metal nanoparticles to the substrate and less contamination (in the case of vacuum evaporated films, hydrocarbon contaminants existing between the metal and the substrate may interfere with the spectral measurements unless the surface is first plasma treated). The adhesion is a relevant property when the deposited island film is used in an electrochemical environment. SEIRA has been extensively used in electrochemistry research with metal films deposited on the silicon prism employed for *in situ* measurements with the Kretschmann attenuated total reflection (ATR) configuration. Particularly, evaporated gold films adhere very poorly to silicon and the standard adhesion promoters have a detrimental effect on their island structure and SEIRA activity. As a result of the efforts made to find new methods for preparation of island Au films with suitable adhesion and enhancement factors, new recipes have been recently published. One of them employs chemical deposition with HF etcher added to the plating solution,[37] and the other is based on etching by aqua regia of a thin Au film initially deposited on the Si prism by thermal evaporation.[42] In both cases, etching of the silicon surface either with HF or with NH_4F solutions to remove oxide layers and to terminate it with hydrogen was carried out. This pretreatment provides enhanced adhesion because it facilitates the formation of a silicide between Si and Au deposits.

Modified SEIRA-active surfaces based on coating the metal substrate with self-assembled monolayers (SAMs) of different thiols have been tested and evaluated, both for gold–silicon[43,44] and for gold–germanium systems.[45] The goal is to extend the applications of the SEIRA technique, making it possible to get some SEIRA enhancement in the case of molecules that, in principle, do not show SEIRA spectra. Such could be the case of molecules without polar groups that, consequently, have no possibility of being chemisorbed to the metallic surface. If the ''modified substrates'' succeed in placing the molecules close enough to the metallic particles for sensing the enhanced electromagnetic field, their infrared spectra would benefit from such enhancement. In particular, sulfur and selenium compounds have a strong affinity to transition metal surfaces and, specifically, SAMs of thiols on gold and silver have been the subject of considerable research because such molecules spontaneously chemisorb to form densely packed and structurally ordered thin films. This fact facilitates the process of obtaining such SAMs modified SEIRA substrates.

Coinage metals Ag and Au, which show high enhancement factors in SERS, have also been the most widely employed metals in SEIRA measurements. However, SEIRA models predict enhancement on transition metals, as strong as on coinage metals.[7] In practice, SEIRA has been observed on many other metals (Cu,[46] Sn,[12] Pb,[47] Fe,[48] Pt,[11] Ni,[49] Pd,[49] Rh,[50] Pt/Ru,[14] Ir,[51] and Pt-Fe alloys[52]), with varying magnitude of enhancement and with some peculiarities affecting the SEIRA band shapes. In fact, while Ag and Au island films lead practically to the

greatest intensity enhancement, SEIRA observed in other metals, specifically the platinum-group metals, shows a modest intensity enhancement and increased band asymmetry. As Pt, Pd, and Rh are very important metals, both because they have been extensively employed as electrode materials for electrochemistry and because they are commonly used as heterogeneous catalysts in a wide variety of industrial processes, their SEIRA enhancer possibilities have been actively explored.[11,13,53] The investigation and explanation through adequate SEIRA models of the abnormal infrared effects (AIREs) observed in the bands of the SEIRA spectra of molecules adsorbed on these metals and on Fe[54,55] is ongoing. It must be mentioned that most metals are easily oxidized in air, forming an oxide layer that affects the local enhanced field.

Several ways of placing the sample under study on the SEIRA-active substrates have been reported. The easiest one is the ''cast film method'' or ''drop-drying method'', in which films of the sample are cast by dropping their dilute solution with a micro syringe over the metallic surface. The solvent is slowly allowed to evaporate, leaving a monolayer film of the sample on the active surface. A thin film of the sample can also be formed by evaporation in vacuum on the metal surface, or formed as a Langmuir film by horizontal deposition in a Langmuir balance and posterior transfer to the SEIRA-active substrate.[9]

When the sample under study is known to chemisorb on the metal of the SEIRA substrate, the ''SAM method'' can be applied. In this case, the SEIRA-active substrate is immersed in a solution of the sample and allowed to soak for some period. Afterwards, the substrate is rinsed thoroughly with the solvent so that a SAM of the sample remains on the metal island surface. In electrochemical environments, the sample is in solution where the roughened electrode (SEIRA-active surface) is used to probe the species adsorbed at the interface.

Transmission Fourier transform infrared (FT-IR) spectroscopy and internal and external reflection have been used in SEIRA measurements. On occasion, diffuse reflection mode has been used for dispersed metallic colloids. However, its use to increase the SEIRA sensitivity for species on the surface of strongly absorbing materials, such as carbon-based catalysts and natural vegetation, is under investigation. For electrochemical studies, ATR-SEIRAS with Kretschmann configuration (a prism/thin metal film/solution) is the best option.[28]

THEORETICAL MODELS FOR SEIRA

The electromagnetic enhancement on rough metal surfaces has been extensively discussed for radiation in both the visible and near-infrared regions of the spectrum,[56] while there has been less work done for the middle- and far-infrared regions. Computational approaches for SERS electromagnetic enhancement (EM)[57,58] are often applicable to SEIRA, and these can be roughly divided into three types: isolated particle models, finite numbers of particle models, and surface and film models.

A simple model for a rough surface is that of a collection of noninteracting spheroids (see reviews and references therein).[4,59,60] For a spheroidal particle, the induced field is uniform, but not necessarily parallel to an arbitrarily applied field, excepting the case of a sphere. The sense of depolarization is that the field inside the particle is less than the applied field, and the term is applied to the induced field. In surface-enhanced spectroscopy, however, the internal field is greater than the applied field. An effort is made to explain the SEIRA effect in terms of surface plasmons in the infrared spectral region.[17] The study used tuned surfaces to give large islands, which have a plasmon resonance in the near to middle infrared. Calculations of field enhancement using the modified long wavelength approximation gave good agreement with observed plasmons on a variety of substrates.[17]

A successful electromagnetic study of enhancement factors in the ultraviolet, visible, and near-infrared regions for a variety of materials showed very weak field enhancement in the near-infrared compared to the visible.[61] This technique can be extended to the full infrared region, although the result should be similar to the static case due to the long wavelengths. We have adapted this method to calculate the field enhancement for silver and tin in the fingerprint region of the infrared and the results are shown in Fig. 1. The model consists of spheroids embedded in a medium of unity dielectric constant, with lengths of 90 and 30 nm for the major and minor axes, respectively. The dielectric functions of the metals are taken from the *Handbook of Optical Constants.*[62] These values for Ag and Sn are plotted in Fig. 2.

Recently, an experimental study of the enhanced infrared absorption of anthracene on dielectric particles, namely SiC and Al_2O_3, reported enhancements on the order of 100 fold.[15] The author argues that this enhancement can be explained on the basis of the surface field enhancements due to phonon resonance. The field enhancements on the surface for these systems can also be calculated. Figure 3 shows the enhancement factor for SiC averaged over the surface of a particle with the same computational parameters as above. The sharpness of the resonance agrees with the argument of phonon contributions, since phonons, compared to plasmons, have much less damping.[63]

Although this model is very useful for giving a prediction of enhancement factors, it neglects the inhomogeneous nature of a film or colloids and also does not account for any chemical contributions to the enhancement. A full discussion of the problems in any electromagnetic calculation in surface-enhanced vibrational spectroscopy can be found in the review by Moskovits.[4]

A more advanced model than that

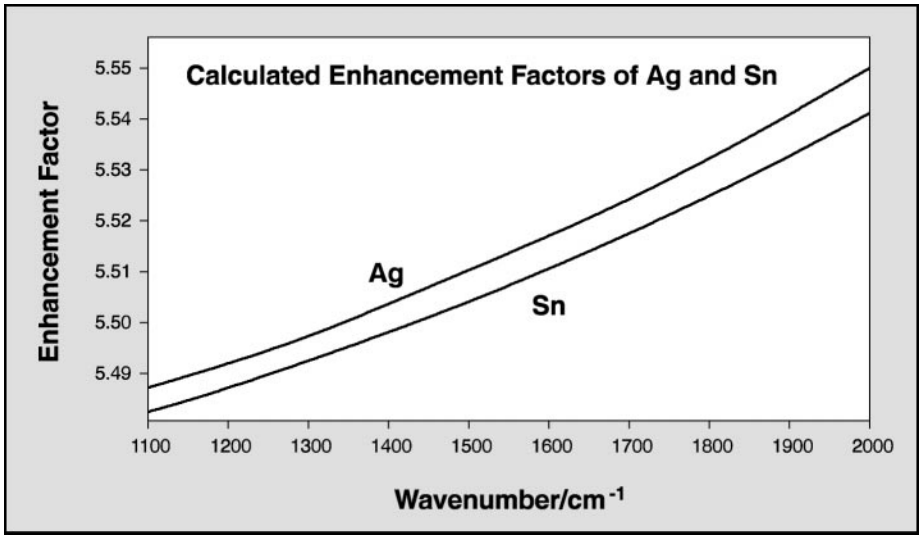

FIG. 1. Enhancement factor calculation for spheroids in vacuum, with lengths of 90 and 30 nm for major and minor axes respectively.

of the isolated particle is a finite number of particles interacting in a well-defined way. Due to the complexity of these calculations, however, their use has not been popular for SERS enhancement calculations and has not been applied to SEIRA.

Effective Medium Theory. The electromagnetic SEIRA enhancement may be calculated using effective medium theories (EMT), which use the effective optical property of a heterogeneous material. The substrates used in SEIRA are usually metal island films or granular materials (such as semi-metals or semiconductors). Effective medium theory is a formalism used to model these discontinuous surfaces so that they may be characterized by a set of effective electrical properties, such as conductivity or dielectric function.[8,9,20,64] In the case of SEIRA the effective property represents an average for the metal films, the substrate, and the organic coat. Finding the dielectric function for the surface-enhanced sample involves finding the effective optical properties of the mixture of these components. The spatial average of the dielectric function of the sample comprising substrate, metal islands, and analyte is achieved using one of the effective medium formalisms.[65–69] A general review, including electrical properties, has been written by Bergman and Stroud.[70]

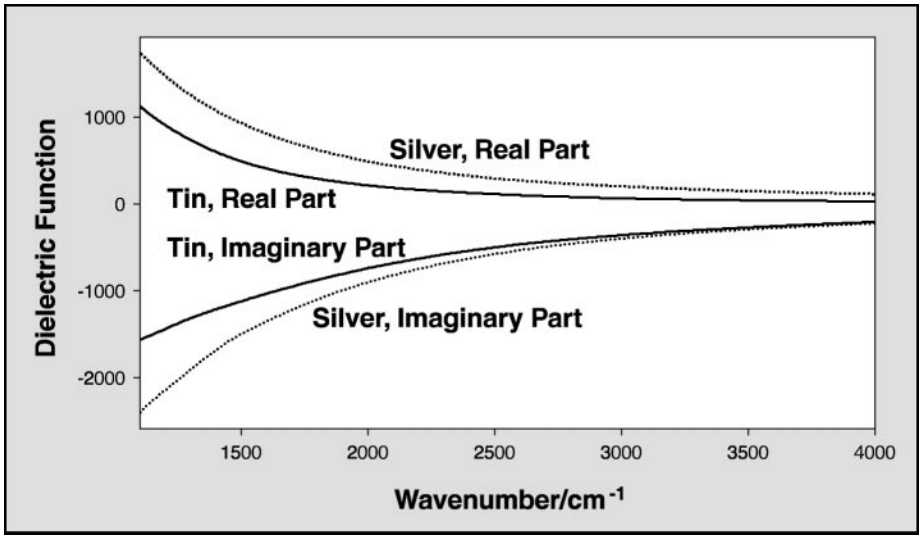

FIG. 2. Real and imaginary parts of the dielectric function for silver (dotted line) and for tin (solid line).

Two of the most used formalisms for effective medium calculations are the Maxwell–Garnet and the Bruggeman methods. The general form of the Maxwell–Garnet model can be given as[67]

$$\bar{\varepsilon} = \varepsilon_h \frac{3 + 2\sum_i f_i \alpha_i}{3 - \sum_i f_i \alpha_i}$$

where α is the polarizability of the inclusions and i is the index over different particles. This allows for the distribution of particle shapes and sizes to be included in the calculation, as opposed to simple spheres. $\bar{\varepsilon}$ is the effective dielectric function, and ε_h is the dielectric function of the host material, in which the particles are embedded, while f represents the volume fraction of the inclusions.

The Bruggeman model is a self-consistent theory that includes a greater amount of interaction between inclusions.[71] The self-consistency enters through the use of the Bruggeman condition, $\varepsilon_h \rightarrow \bar{\varepsilon}$, which requires that the solution be a dielectric function of a host that has the same optical properties as the effective medium. This formalism can be expressed in general as

$$\bar{\varepsilon} = \varepsilon_h \frac{3(1 - f) + f\alpha'}{3(1 - f) - 2f\alpha'}$$

where α' is the polarizability of the inclusions with the ''Bruggeman'' condition applied.

There are several reports in which EMTs have been used to model SEIRA experiments.[9,11,64] Osawa[7] models island films as a set of ellipsoids of rotation, where the symmetry axis is normal to the substrate. In the present calculations, the polarizability of a coated ellipsoid is used, with depolarization factors derived by Ston-

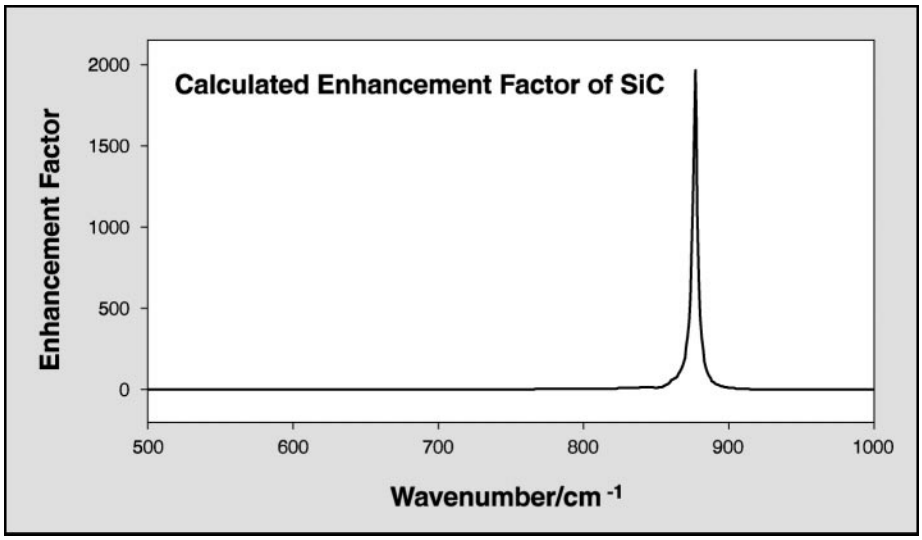

FIG. 3. Enhancement factor for SiC averaged over the surface of a particle with the same computational parameters as those in Fig. 1

er.[72] Since the inhomogeneities in the layer are much smaller than the wavelength of the incident light, it is assumed that the mixed film is a continuous, parallel-sided layer, so Fresnel's equations may be used to calculate the reflectance and transmittance.[73] In general, discontinuous metal films consist of islands, which may be modeled as ellipsoids of revolution or spheroids of uniform shape and size.[68] There are two different types of ellipsoids of revolution: oblate, where the two larger axes are equal, and prolate, where the two smaller axes are equal. Normann et al.[67] claim that prolate spheroids with the rotation axis parallel to the plane provide the best description of electron micrographs as well as the best fit between measured and computed spectra.

The dielectric function, denoted ε_m, for the bulk metals was taken from the *Handbook of Optical Constants of Solids.*[62] Islands have a major axis of length a, minor axis b, and an aspect ratio defined as $\eta = a/b$. A geometry for the metal islands can be found by fitting computed UV-Visible plasmon spectra to measured data in the same region. The characteristic plasmon resonances for metals in this region lead to strong absorption bands for most noble metals, and these spectral features are strongly dependent on the shape and size of the metal particles.

Additional considerations of the inhomogeniety of the size and shape of the particles can be taken into account by using a distribution. Since real films are not made up of surfaces with particles of only one size and aspect ratio, a distribution of the axis of particles that make up a film makes a better model for the surface.[67] It has been found that a log-normal distribution provides the best fit for electron microscopy data.[74] The log-normal distribution is given by:

$$f_{LN}(x_s) = \frac{1}{(2\pi)^{1/2}\ln(\sigma_s)}\exp\left\{-\frac{1}{2}\left[\frac{\ln(x_s/\bar{x}_s)}{\ln(\sigma_s)}\right]^2\right\}$$

Where σ_s is the standard deviation of the length of the minor axis, x_s is the length of the minor axis, and $\bar{x}_s$ is the average length of the minor axis. In general, a larger deviation will result in a broader plasmon, since contributions from many different shapes will form the spectra.

The introduction of the organic layer to the metal surface can be represented in two ways. The first is to assume that the molecule forms a thin layer uniformly coating the surface. The net dipole moment p may be given by[73,75]

$$p = \alpha V E_{loc}$$

where α is the polarizability, V is the volume of the inclusion, and E_{loc} is the local field, made up of the incident field and the enhanced field from the particle. For a coated spheroid with one axis parallel to the incident electric field, the polarizability is given by[75,76]

$$\begin{aligned}\alpha = \sum_i \frac{1}{2}\big(\{&(\varepsilon_d - \varepsilon_h)\\ &\times [\varepsilon_m L1_i + \varepsilon_d(1 - L1_i)]\\ &+ Q(\varepsilon_m - \varepsilon_d)\\ &\times [\varepsilon_d(1 - L2_i) + e_h L2_i]\}\\ \div \{&[\varepsilon_d L2_i + \varepsilon_h(1 - L2_i)]\\ &\times [\varepsilon_m L1_i + \varepsilon_d(1 - L1_i)]\\ &+ Q(\varepsilon_m - \varepsilon_d)(\varepsilon_d - \varepsilon_h)\\ &\times L2_i(1 - L2_i)\}\big)\end{aligned}$$

where ε_m is the dielectric function of the metal, ε_d is the dielectric function of the organic layer, and ε_h is the dielectric function of the host medium. Q is the volume ratio of the ellipsoid, defined by $Q = V_{core}/V_{coat}$, i is the index over the axes of the inclusion, and $L1_i$ and $L2_i$ are the geometrical factors corresponding to the core ellipsoid and the coated ellipsoid, respectively.

Basic to the definition of ellipsoids is the geometrical factor. The geometrical factor is a measure of the curvature perpendicular to a specific axis of the ellipsoid and has a value $0 < L < 1$. The geometrical factors for the major axis of an oblate are[68]

$$L_1 = \frac{g(e)}{2e^2}\left[\frac{\pi}{2} - \tan^{-1}g(e)\right] - \frac{g^2(e)}{2},$$

$$g(e) = \left(\frac{1 - e^2}{e^2}\right)^{1/2}$$

And for the major axis of a prolate

$$L_1 = \frac{1 - e^2}{e^2}\left(-1 + \frac{1}{2e}\ln\frac{1 + e}{1 - e}\right)$$

where e is the eccentricity of the spheroid.

The second method of introducing organic molecules to the metal surface is to model the inclusions di-

rectly embedded in the organic matrix. This model is better suited to thicker layers of organic, since a coating around a particle poorly describes this case. In this model the polarizability is given by

$$\alpha = \sum_i \frac{1}{2} \frac{\varepsilon_m - \varepsilon_d}{\varepsilon_d + L_i(\varepsilon_m - \varepsilon_d)}$$

with the same notation as above, excepting that only one geometrical factor is needed.

For the Bruggeman EMT, the Bruggeman condition is also applied to obtain α'.[7] The reaction field equations are used for both the Maxwell–Garnet and the Bruggeman theory and use coated ellipsoid polarizability as outlined above for application to SEIRA calculations.

The Bruggeman EMT tends to give higher enhancements and has often been used to explain some of the larger experimentally observed enhancements. However, these experiments also used molecules that chemisorbed, and so some of the observed enhancement may be due to the chemisorption of the molecule onto the surface.[69]

Effective medium theory is a popular model for SEIRA as enhancement factors can be calculated without any difficulties regarding the nature of the enhancement. Although useful, effective medium theory does not give any insight as to the mechanism of the phenomenon.

As an example of effective medium calculations in use, Fig. 4 shows the Maxwell–Garnet calculation for a collection of prolate ellipsoids, with a major axis of 90 nm and a minor axis of 30 nm, and uniformly coated with a 1 nm thick layer of the analyte. The analyte in these model calculations is 3,4,9,10-perylene-tetracarboxylic-dianhydride, or PTCDA, a well-known organic dye.[77] The dielectric function for the organic is taken from the absorption using a Lorentz model using the 1300 cm^{-1} band of PTCDA and applied as a constant across the whole range of the calculation, giving the effect of the metal. The result is very similar to those of the field calculations from a single particle, increasing towards the visible range of the spectrum, but the enhancement for tin is slightly higher than for silver in this case.

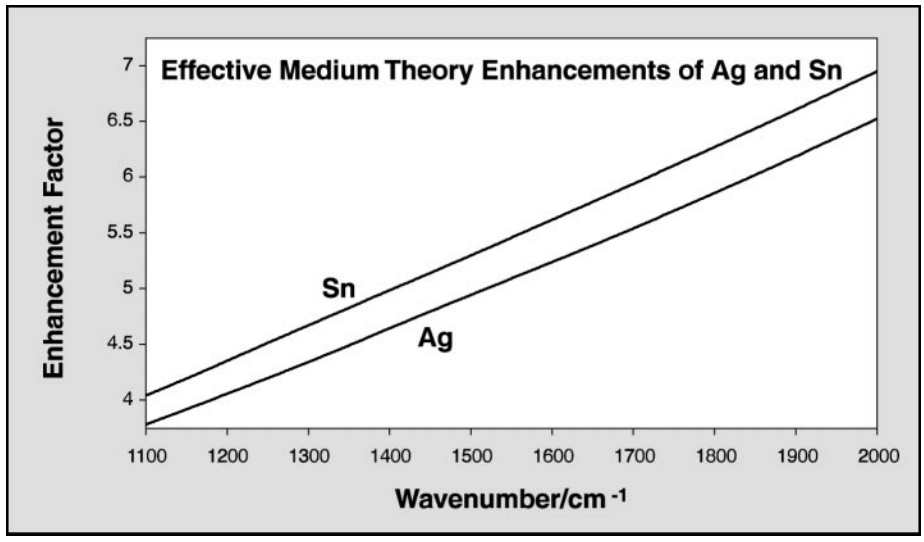

FIG. 4. Maxwell–Garnet computation for a collection of prolate ellipsoids, with a major axis of 90 nm and a minor axis of 30 nm, coated with a 1-nm-thick layer of PTCDA.

SPECTRAL INTERPRETATION AND SELECTION RULES: STUDY CASE

Determining whether the absorption of electromagnetic radiation by an oscillating dipole is possible leads to the *electric dipole selection rules*, and it is found that the probability of the absorption is proportional to the square of the transition dipole moment element along the photon polarization.[78] In particular, the description of the absorption of light by an oscillating molecule in the ground electronic state requires knowledge of the coupling of the dielectric dipole to an external electromagnetic field: $H' = -\mu \cdot E$.[79] The probability for the absorption is thus proportional to the square of the dipole moment matrix element along the direction $\mathbf{E_j}$ of light polarization. The amplitude of the transition is proportional to the scalar product $j \cdot \langle \psi_0 | \mu | \psi_1 \rangle$, where the wave functions are those of the harmonic oscillator.[80,81] In the gas phase, where all molecular orientations have equal probability, the geometrical part of the scalar product is a constant. Therefore, the selection rules for fundamental transitions between vibrational levels ψ_0 and ψ_1 are determined by the matrix element $\langle \psi_0 | \mu | \psi_1 \rangle$. Since we are discussing the ground electronic state, the dipole moment μ is a function of the vibrational coordinates and for infinitesimal vibrations it can be written in a Taylor series. The series for one generalized coordinate has the form

$$\mu = \mu_0 + \left(\frac{\partial \mu}{\partial Q_k}\right)_0 Q_k + \frac{1}{2}\left(\frac{\partial^2 \mu}{\partial Q_k^2}\right)_0 Q_k^2 + \cdots$$

The integral for the first term is zero. In the electrical harmonic approximation, the third term is neglected, and the harmonic vibrational intensities for the k fundamental vibrational mode is determined by the integral

$$\left\langle \psi_0 \left| \left(\frac{\partial \mu}{\partial Q_k}\right)_0 Q_k \right| \psi_1 \right\rangle \quad \text{or}$$

$$\left(\frac{\partial \mu}{\partial Q_k}\right)_0 \langle \psi_0 | Q_k | \psi_1 \rangle$$

In Cartesian coordinates the dipole moment derivative is a vector $\mu' = \mu_x' + \mu_x' + \mu_x'$ with components μ_i'. In the ground electronic state, the equilibrium geometry determines the

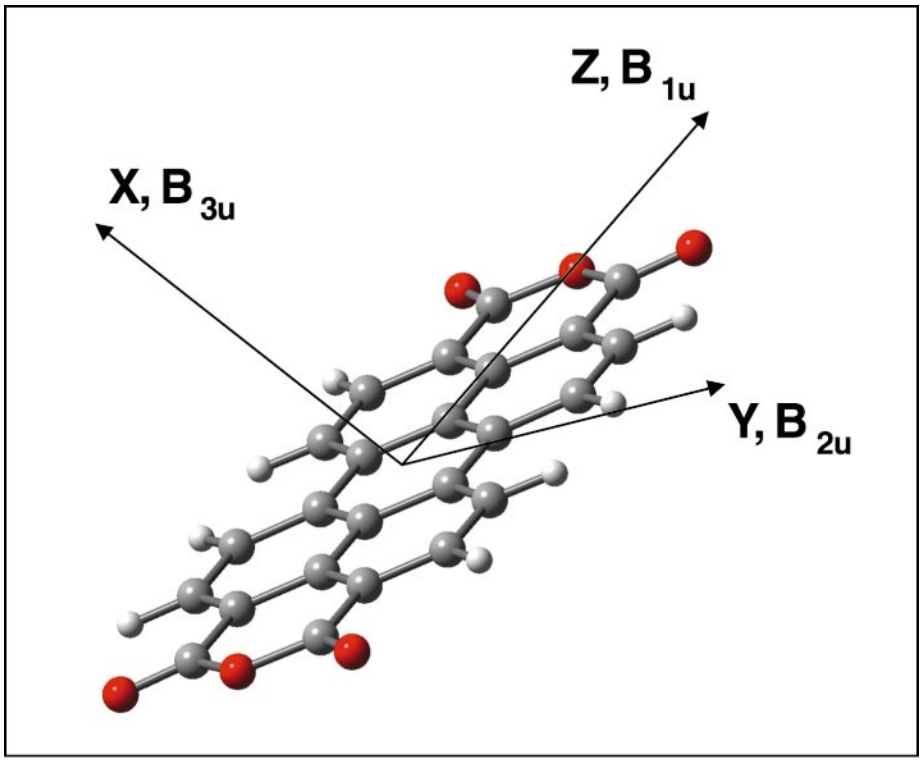

FIG. 5. Planar, D_{2h} PTCDA molecule.

symmetry point group of the molecule, simplifying the application of selection rules by including the vector components different from zero in the character table of each point group. Symmetry reduces the electric dipole selection rules for an allowed transition between two vibrational states, connected by an operator, to the requirement that the direct product (triple product) has a totally symmetric component (p. 128 of Ref. 82). For an isolated molecule or gas-phase spectra, the triple product is directly given in the character table.

In the solid state or for molecules with a fixed spatial orientation, the intensity of a vibrational transition would be proportional to $(E\cdot\mu_i)^2$, where μ_i' is the component of the dynamic dipole in the direction i of the optical field **E**. Therefore, for allowed infrared modes of a given symmetry species to be seen with maximum vibrational infrared absorption intensity, there must be alignment between the polarization of electric field vector **E** and one of the non-zero components of the dynamic dipole moment derivative. On reflecting metal surfaces, the incident and the reflected electric field vectors form the plane of incidence. Electromagnetic waves with the electric field normal to the plane of incidence are denoted as *s*-polarized, transverse electric (TE), or ⊥ waves. When the electric field is parallel to the plane of incidence a wave is called *p*-polarized or transverse magnetic (TM). In 1966, Greenler[83] studied adsorbed molecules on metal surfaces by reflection techniques realizing that at high angles of incidence, *p*-polarized light ''have a sizable component of the electric vector normal to the metal surface''. The opposite is true for the *s*-polarized light. Therefore, for molecules adsorbed onto metal surfaces the vibrational intensity is derived from $(E_j\cdot\mu_i)^2$. The latter amounts to adding further constraint to the selection rules of the free molecule: the alignment of dipole moment derivative with the light polarization. For molecules adsorbed onto reflecting surfaces where light is polarized with the electric vector perpendicular to the reflecting surface, the new rules are called *surface selection rules.*

The reduction of the surface selection rules for metal surfaces to the statement ''that only the vibrational modes having nonzero dipole moment derivative components perpendicular to the surface were infrared active'' was also advanced by Pearce and Sheppard[84] and Hexter and Albrecht,[85] explaining the observation in terms of the induced image dipoles. A dipole moment change parallel to the surface is cancelled by a dipole moment change of the same magnitude in the opposite direction, induced in the substrate, while dipole moment changes perpendicular to the surface are reinforced and the total dipole moment would be doubled.

As a study case to illustrate the application of the selection rules in the spectral interpretation of the FT-IR transmission, reflection–absorption infrared spectroscopy (RAIRS), and SEIRA, we have selected the 3,4,9,10-perylene-tetracarboxylic-dianhydride (PTCDA) dye, a molecule with 38 atoms ($C_{24}H_8O_6$), 108 vibrational degrees of freedom, and 46 infrared active fundamental vibrations[86] distributed in $10b_{3u}(x) + 18b_{2u}(y) + 18b_{1u}(z)$ symmetry species. The molecule is a flat rectangle of 14.2 Å for the long axis (z) and 9.2 Å on the short axis (y) as shown in Fig. 5.

Since the molecule has a center of symmetry (D_{2h} group), the mutual exclusion rule applies. RAIRS is an infrared technique that takes advantage of the large E_j component at the reflecting surface. In the present study case the samples for RAIRS were prepared by first evaporating 100 nm of Ag onto a Corning 7059 glass slide, held at 200 °C under high vacuum. Fifty nanometers of perylene tetracarboxylic anhydride (PTCDA) were then evaporated onto this smooth silver surface.[87] The RAIRS spectra are obtained by using a Spectra-Tech variable angle reflectance accessory set such that the incident beam impacted the surface at 80° from the normal.

The reference is the transmission

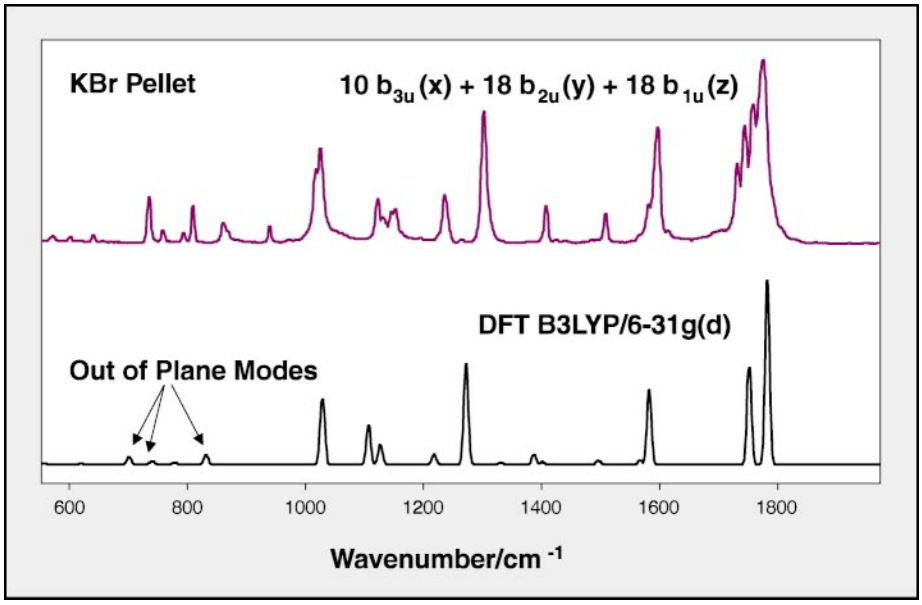

FIG. 6. FT B3LYP/6–31g(d) computation results, and the transmission FT-IR spectrum of PTCDA in a KBr pellet.

spectrum of the solid dispersed in a KBr pellet that is equivalent to a random distribution of the PTCDA molecules, i.e., a random molecular orientation. To help the vibrational analysis a calculation of the vibrational frequencies and intensities is carried out. To illustrate the agreement between the experiment and density functional theory (DFT) computations, the transmission FT-IR of a PTCDA pellet and the B3LYP/6-31g(d) results obtained using Gaussian 98,[88] where a scaling factor of 0.9614[89] was used, are shown in Fig. 6. It can be seen that there is a good agreement between the calculated and observed vibrational intensities. The latter is in spite of the condensed matter effects on the observed infrared spectra and the fact that the computations are performed within the harmonic approximation. The spectrum of the KBr pellet can now be compared with the RAIRS spectrum of a 50 nm PTCDA film deposited onto a smooth reflecting silver mirror. The RAIRS results are shown in Fig. 7, where the calculated vibrational intensities for the b_{3u} species are also included to facilitate the assignment. According to the surface selection rules, only the vibrational modes having nonzero dipole moment derivative components perpendicular to the surface should be active in RAIRS. Hence, from the RAIRS spectrum of the PTCDA molecule it can be extracted that it is preferentially oriented with its x-axis (out-of-molecular plane) perpendicular to the metal surface, a flat-on molecular orientation. Similar results were obtained for PTCDA films of 20 nm mass thickness.[87] The fact that the in-plane vibrations are still seen is an indication that in this relatively thick film (50 nm mass thickness) there is a certain degree of randomness.

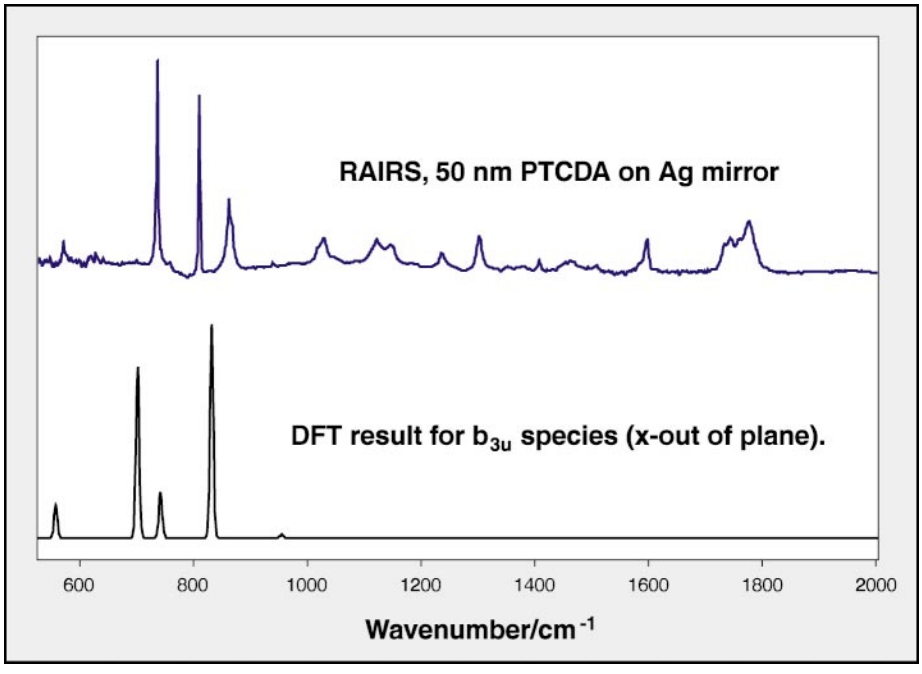

FIG. 7. RAIRS spectrum of a 50 nm PTCDA film deposited onto a smooth reflecting silver mirror and calculated vibrational intensities for the b_{3u} species.

The SEIRA spectrum was also obtained by depositing a 50 nm PTCDA film onto a silver island film (15 nm mass thickness of Ag), for which an atomic force microscopy image and the corresponding plasmon absorption are shown in Fig. 8. The experimental conditions for the deposition of the SEIRA metal surface are the same as for the RAIRS experiment, except, of course, for the mass thickness. The spectroscopic results for a 50 nm mass thickness PTCDA film deposited on silver islands and on a KBr crystal are shown in Fig. 9. For comparison, the spectra of the KBr pellet is included as a reference. If one assumes the same molecular orientation in the PTCDA films deposited onto smooth silver film and KBr crystal, the transmission spectrum of the film on

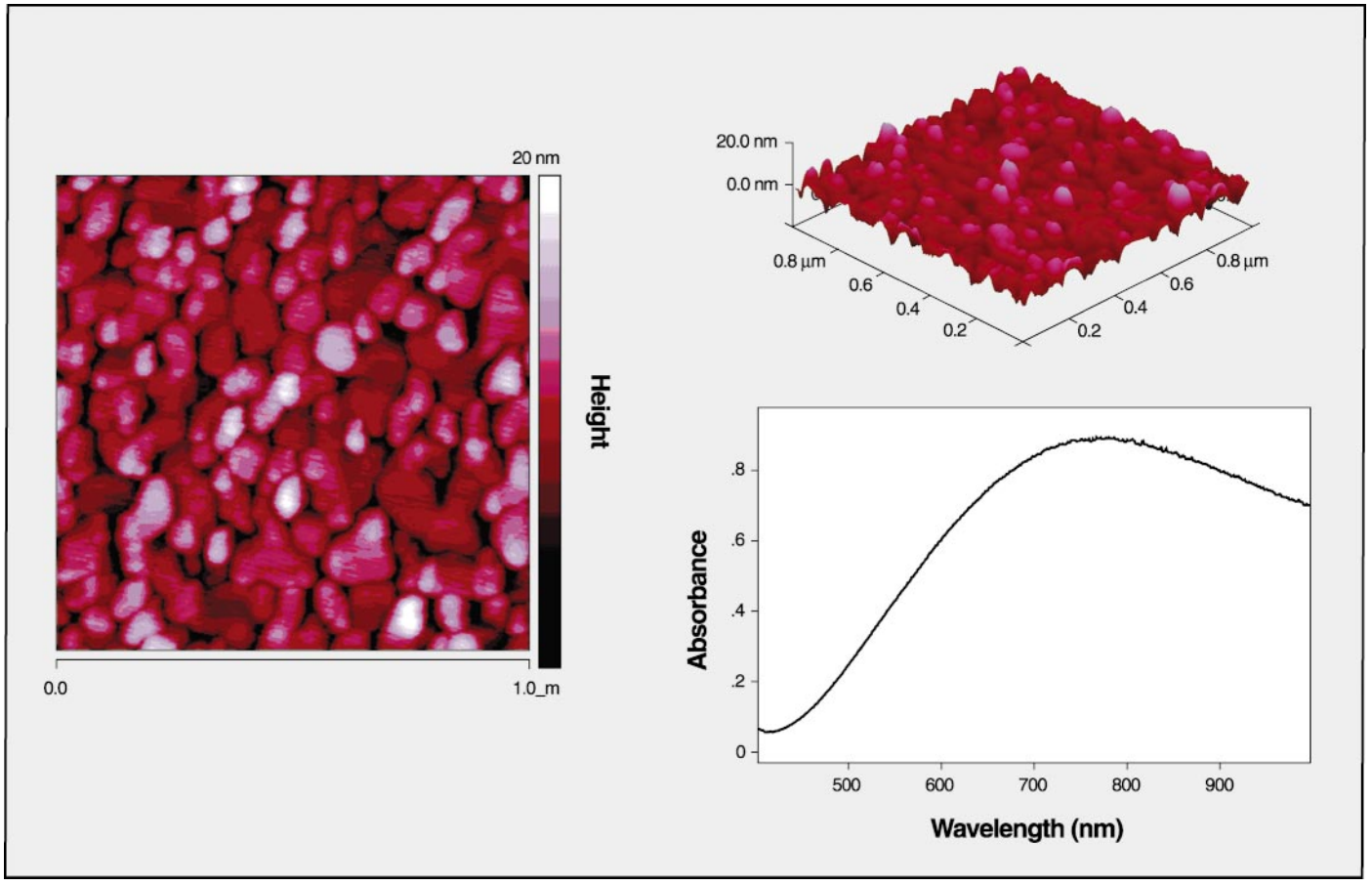

FIG. 8. AFM image and UV-Visible absorption spectrum of a 15 nm evaporated Ag film.

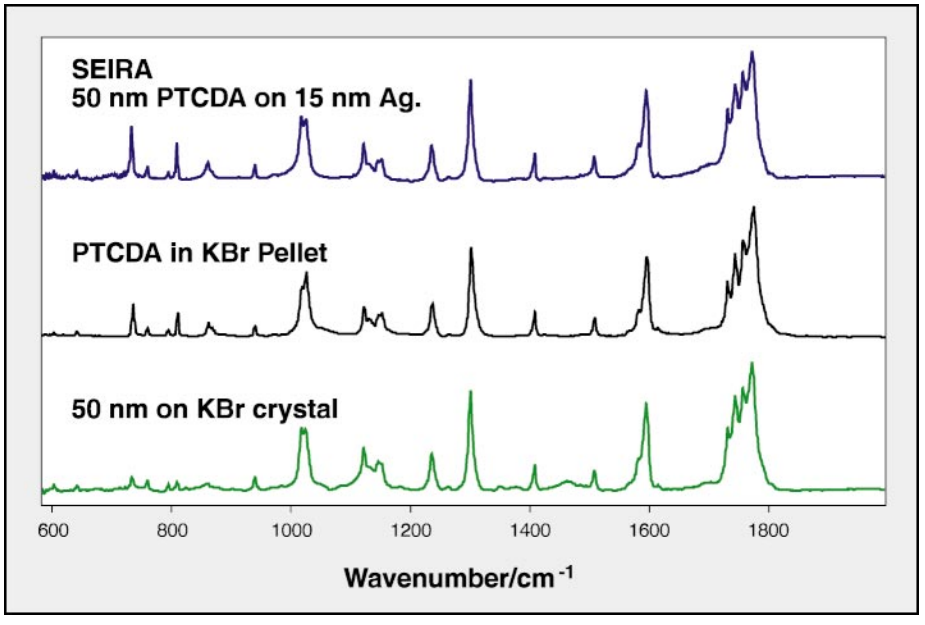

FIG. 9. Transmission spectra of a PTCDA pellet, SEIRA spectrum, and a 50 nm film on KBr crystal.

KBr, where the electric field is polarized parallel to the surface, should give a strong absorption for the in-plane mode and a weak signal for the out-of-plane modes (b_{3u}). Since the latter is observed (Fig. 9), the transmission spectrum of the PTCDA film on the KBr crystal is in agreement with the RAIRS results, pointing to a preferential flat-on molecular orientation in the evaporated films. The SEIRA spectrum shown in Fig. 9 is strikingly different from the RAIRS spectrum and clearly does not show the same selection rules. Since in the infrared spectral region one would also expect the local optical field on the surface of the silver island film to be perpendicular to the surface (as in RAIRS), the simplest explanation would be to assume that the PTCDA molecules are not oriented flat-on the metal island, and instead there is a random distribution of orientations and the vibra-

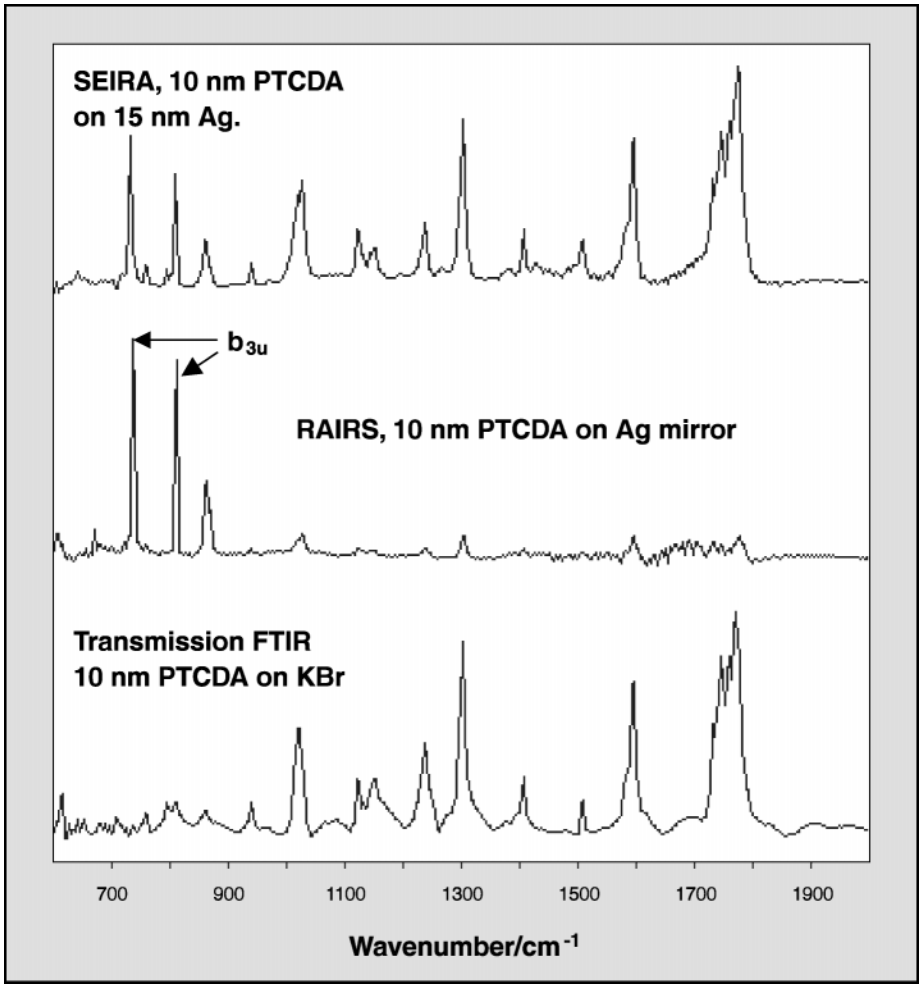

FIG. 10. SEIRA spectrum of the 10 nm PTCDA film on a 15 nm silver island film, RAIRS spectrum of the 10 nm PTCDA film on a smooth silver mirror, and transmission FT-IR spectrum of the 10 nm PTCDA film on KBr crystal.

tional intensities are much closer to that of the free molecule (or KBr spectrum).

Since the films used in the previous experiments were relatively ''thick'', we repeated the experiments using a PTCDA film of 10 nm mass thickness. The transmission spectrum of the neat PTCDA film on the KBr crystal and the SEIRA spectrum of the 10 nm PTCDA film on a 15 nm silver island film were recorded under identical experimental conditions using the Bomem DA3 vacuum bench instrument. The RAIRS spectrum of the 10 nm PTCDA film on a smooth silver mirror was recorded in the Bruker instrument with *p*-polarized light. The results are shown in Fig. 10. It can be seen that the selection rules observed in the RAIRS spectrum unmistakably point to a flat-on molecular orientation of PTCDA with a strong relative intensity for the out-of-plane b_{3u}. Notably, the SEIRA spectrum does not follow the RAIRS pattern. However, the relative intensity of the out-of-plane modes has increased with decreasing film thickness, hinting at a proportional increase of PTCDA molecules oriented flat-on the silver islands.

The PTCDA case presented here is of interest for researchers trying to extract molecular orientation information using SEIRA. In such cases it is advisable to carry out the RAIRS experiments[90,91] with the same species as a reference point for the SEIRA results. In conclusion, the observation of strict adherence to surface selection rules in RAIRS may not be mimicked by the SEIRA spectrum.

APPLICATIONS OF SURFACE-ENHANCED INFRARED ABSORPTION

Surface-Enhanced Infrared Absorption of Ultrathin Films. The SEIRA technique, as well as SERS, is a powerful tool for structural characterization of ultrathin films and well-ordered monolayers on metal surfaces. Thin films at interfaces are prepared with different procedures and developed for various applications. The fabrication and characterization of ultrathin films is an exciting area of research[28,92,93] in which some of the most interesting subjects are: (1) bilayers and monolayers at a liquid–liquid interface; (2) adsorption monolayers and Langmuir (water-insoluble) monolayers at an air–water interface; (3) adsorption films and self-assembled monolayers (SAMs) at a liquid–solid interface; and (4) Langmuir–Blodgett films, cast (deposit) films, and spin-coat films at an air–solid interface. The molecular organization in these thin films depends on the conditions of preparation and can be extracted using vibrational techniques. Among the many SEIRA applications to films and interfaces one finds studies about the molecular organization of monolayers of porphyrin derivatives,[94,95] of azamacrocycles, and of their metallic derivatives[96,97] at the air–solid interface. Dendrimers architectures adsorbed on SAMs modified gold surfaces have also been investigated using SEIRA.[98,99] Similarly, bifunctional molecules that have interesting technological applications are also among the SEIRA targets. For instance, adlayers of 2,2′-Bypiridine have been formed with electrochemical techniques on Cu and investigated with SEIRA at solid–liquid interfaces.[100] These molecules could work as molecular electric devices, as their reversible orientation can be controlled by electrode potentials. The electrochemical adsorption

of 4,4′-Bypiridine (4,4′-BP), its phase behavior, and its coadsorption with interfacial water on gold (thin film) electrodes has been studied using *in situ* SEIRA and *ex situ* scanning tunnel microscopy (STM).[101] The 4,4′-BP bifunctional nonchelating ligand acts as a bridging spacer and coordination unit in three-dimensional and/or two-dimensional supramolecular lattices with novel electric and magnetic properties.

Recently, characterization using surface-enhanced vibrational spectroscopy, SEIRA, and SERS has begun to emerge as demonstrated in the study of nanoarrayed superstructures formed by adsorption of 1,4-phenylene diisocyanide (1,4-PDI) on gold nanoparticles.[102] 1,4-PDI is adsorbed on gold via the carbon lone-pair electrons of one isocyanide group assuming a vertical orientation with respect to the gold substrate. The pendent isocyanide group is further identified by SEIRA, AFM, and QCM to react with Au nanoparticles. The SEIRA spectroscopy also revealed that 1,4-PDI molecules could be newly adsorbed on those Au nanoparticles, implying that nanoarrayed electrodes could be fabricated using 1,4-PDI as the conducting wires of Au nanoparticles.

Surface Photochemistry and Catalytic Reactions. Given the catalytic activity of some metal particles, SEIRA is a new analytical tool in catalysis. SEIRA has been successfully used to help explain the photoenhanced hydrophilicity of the photocatalyst TiO_2,[103] and later SEIRA was applied to *in situ* observation of surface products during the photooxidation of gas-phase n-decane on TiO_2 films coated with Au[104] and Pt.[105] Similarly, the photocatalytic decomposition of acetic acid, both in liquid and vapor phase, using TiO_2 has been investigated in SEIRA.[106] The feasibility of *in situ* ATR-SEIRA spectroscopy for the study of liquid-phase heterogeneous catalysis by platinum metals has also been reported.[107]

Electrochemistry. Further, SEIRA, most commonly done using the ATR Kretschmann configuration, is a successful *in situ* surface-sensitive technique for electrochemical dynamics studies, and several reviews on such applications have been published.[28,108] A discussion on the practical advantages of the ATR Kretschmann configuration in electrochemistry can be found in Ref. 28. In summary, free mass transport, less interference from the solution, and higher sensitivity owing to SEIRA enhancement give SEIRA a unique high sensitivity for infrared measurements on time scales of fast cyclic voltammetry. Indeed, the time resolution for measurements of CO adsorbed on Pt is in the range of μs with the use of a step-scan interferometer, with a sensitivity 30–75 times higher than with conventional IR spectroscopy, including the effect of enhancement due to the rough electrode, which is of the order of seven.[109] Furthermore, thanks to developments in FT-IR instrumentation and data analysis techniques such as 2D-IR, SEIRA has enabled the study of electrode dynamics that are not readily accessible by conventional electrochemical techniques.[110] Recently, thanks to the SEIRA advantages, formate has been detected, for the first time, as an active intermediate species in the non-CO pathway of the electro-oxidation of methanol on platinum electrodes.[111] Although the catalytic electro-oxidation of methanol (and methane) on Pt or Pt based metal electrodes had been extensively studied due to their potential use in low-temperature fuel cells, the detection of formate strongly suggests that many previous reaction mechanisms may have to be reconsidered. SEIRA experiments have also helped to show that formate is the active intermediate in the electro-oxidation of formaldehyde on Pt electrodes.[112] *In situ* SEIRA studies on the anodic oxidation of methane at Pt, Au, Pd, Ru, and Rh electrodes[13] have revealed that it is possible to activate methane at room temperature using noble metals as electrocatalysts, and that Pt and Ru seem to be the most active ones for such purpose.

Analytical Applications. The SEIRA technique is a surface-sensitive spectroscopy that has the great advantage of profiting from a vast body of vibrational data, collected, understood, and classified in libraries for all three states of matter. In addition, a modest enhancement factor (10–100) makes IR spectroscopy an attractive and powerful analytical tool. The cross-sections of infrared absorption are an order of magnitude larger than Raman cross-sections. For instance, the cross-section σ for absorption in the infrared is approximately 10^{-20} cm^2. The absolute Raman cross-section for the 666 cm^{-1} mode of chloroform has been determined,[113] using the 532.0 laser line, to be $\sigma_R = 0.660 \pm 0.1 \times 10^{-28}$ cm^2. Therefore, the sensitivities of ''average'' SERS and SEIRA are comparable and both are presently under development as promising ''optical sensor technologies''.

The analytical application of SEIRA as a surface-sensitive spectroscopy requires a thorough examination of metal–molecule interactions and polarization effects that may give rise to a distinct vibrational spectrum, in many cases, quite different from that of the parent molecule. Peak positions and relative intensities in the enhanced spectra may be different from those of normal spectra of the same molecules, and the deviation is larger for strongly chemisorbed adsorbates. The latter means that the databases of normal IR spectra cannot be used directly for automatic identification of compounds through their SEIRA spectra and that new databases must be built. The enhancement is short range, being most effective for molecules on or near the metal surface, and therefore, the band intensity in SEIRA is not a linear function of the amount of molecules.

In trace analysis, SEIRA has been used as a detector for flow-injection systems and applied in the analysis of environmentally hazardous chemicals in waste water.[29] Recently, good results have been reported by coupling SEIRA to liquid chromatography (LC)[114] and to gas chromatography (GC), employing silver islands

on ZnSe as SEIRA-active surfaces.[115] Detection limits ten times lower in comparison with GC-FTIR have been reported for chemisorbed molecules. As an immediate objective, the equipment for GC- and HPLC-SEIRA recently developed in Griffiths's group will be tested for the analysis of drugs in hair, as an alternative to urinalysis.

Thiram and ziram, two dithiocarbamate fungicides of potential aggressive environmental impact, have been the subject of concurrent SEIRA and SERS studies, using the same ''enhancing substrate''.[116] For these compounds, SEIRA is the preferred enhanced technique. There are also several biological applications reported using SEIRA, and it has been tested for various bioanalytical purposes including immmunoassays.[32,117] Biosensors use antibodies or enzymes, immobilized on a platform, to interact selectively with antigens or substrates, and then one of several possible transduction mechanisms to detect that interaction. The reported SEIRA based biosensors have used colloidal gold to immobilize antibodies for *Salmonella*[32] and for staphylococal protein A,[117] employing external reflection and ATR techniques, respectively. In a different application, SEIRA microspectroscopy was used for localization of bacteria on geologic material surfaces and their ulterior investigation.[118] In that case, gold was evaporated on the samples.

Relevant information about the adsorption and orientation of nucleic acid bases on metal surfaces have been obtained from SEIRA studies of thymine on silver island films,[119] cytosine,[120] and uracil[121] on gold electrodes. On the other hand, SEIRA studies of the structure of nucleic acids and phospholipids from tumor cells, both drug-sensitive and drug-resistant ones,[122–124] seem to have opened new expectations about the possibility of using SEIRA as diagnostic criteria in cancer research. The reason is that this method enhances a set of bands that are impossible to observe in conventional IR spectroscopy, but that are crucial for determining nucleic acid structural peculiarities from tumor tissues and nucleic acid interactions with anticancer drugs. SEIRA data about DNA interaction with single-walled carbon nanotubes (SWCNT)[125] could be explained by the previously proposed model of the wrapping of nucleic acid molecules around carbon nanotubes. This is an interesting result because a similar situation seems to occur in chromosomes during DNA assembling by histones.

Adsorption of protein rich vesicles onto Ag cluster coated Ge crystals in an aqueous environment has been investigated with SEIRA.[126] The nicotinic acetylcholine receptor, the structurally best-characterized prototype of the ligand-gate neuroreceptor, was the membrane protein contained in the vesicles. The SEIRA technique has thus allowed the detection of small and specific changes in the structure of biomembranes, changes practically impossible to detect by normal FT-IR spectroscopy.

The electrochemically induced oxidation and reduction process of a monolayer of horse heart Cytochrome C, a protein that mediates single-electron transfer between the integral membrane protein complexes of the respiratory chain, has been followed by SEIRA.[127] In this case the SEIRA-active substrate was rough gold modified with a SAM of mercaptopropionic acid (MPA). The results obtained demonstrate that minute enzymatic changes of a protein can be studied on the level of a monolayer using SEIRA. SEIRA has been applied in the analysis of plasma-modified polymer surfaces[128] and in the study of the adhesion mechanisms of functional monomers used for the surface treatment of dental alloys on the basis of their molecular structural information.[129] Other interesting materials, fullerenes, have also been explored with SEIRA.[130]

Surface-enhanced infrared absorption is an integral part of the surface-enhanced vibrational spectroscopy and the complement of SERS. The enhancement factors in the absorption are very modest in comparison with SERS. However, infrared absorption cross-sections are already orders of magnitude higher than the corresponding Raman cross-sections, and a modest increase could have an enormous effect in practical applications. The vast body of infrared data guarantees a broad range of analytical applications and in particular its own development as a surface analytical technique.

ACKNOWLEDGMENTS

Financial assistance from the NSERC and SHARCNET of Canada is gratefully acknowledged. C.D. acknowledges the Ministerio de Ciencia y Tecnología, MCYT, of Spain for financial assistance under Project BFM2001-2265, and Drs. García-Ramos and Sánchez-Cortés for discussions and encouragement.

1. D. L. Jeanmaire and R. P. Van Duyne, J. Electroanal. Chem. **84,** 1 (1977).
2. M. G. Albrecht and J. A. Creighton, J. Am. Chem. Soc. **99,** 5215 (1977).
3. M. Fleischmann, P. J. Hendra, and A. J. McQuillan, Chem. Phys. Lett. **26,** 163 (1974).
4. M. Moskovits, Rev. Mod. Phys. **57,** 783 (1985).
5. K. Kneipp, H. Kneipp, I. Itzkan, R. R. Dasari, and M. S. Feld, Chem. Phys. **247,** 155 (1999).
6. A. Hartstein, J. R. Kirtley, and J. C. Tsang, Phys. Rev. Lett. **45,** 201 (1980).
7. M. Osawa, Bull. Chem. Soc. Jpn. **70,** 2861 (1997).
8. Y. Nishikawa, K. Fujiwara, K. Ataka, and M. Osawa, Anal. Chem. **65,** 556 (1993).
9. E. Johnson and R. Aroca, J. Phys. Chem. **99,** 9325 (1995).
10. R. Kellner, B. Mizaikoff, M. Jakusch, H. D. Wanzenbock, and N. Weissenbacher, Appl. Spectrosc. **51,** 495 (1997).
11. A. E. Bjerke, P. R. Griffiths, and W. Theiss, Anal. Chem. **71,** 1967 (1999).
12. R. Aroca and B. Price, J. Phys. Chem. B **101,** 6537 (1997).
13. F. Hahn and C. A. Melendres, Electrochim. Acta **46,** 3525 (2001).
14. M. S. Zheng, S. G. Sun, and S. P. Chen, J. Appl. Electrochem. **31,** 749 (2001).
15. M. S. Anderson, Appl. Phys. Lett. **83,** 2964 (2003).
16. P. C. Andersen and K. L. Rowlen, Appl. Spectrosc. **56,** 124A (2002).
17. T. R. Jensen, R. P. Van Duyne, S. A. Johnson, and V. A. Maroni, Appl. Spectrosc. **54,** 371 (2000).
18. A. Otto, I. Mrozek, H. Grabhorn, and W. Akemann, Condens. Matter **4,** 1143 (1992).
19. A. Campion and P. Kambhampati, Chem. Soc. Rev. **27,** 241 (1998).
20. D. Ross and R. Aroca, J. Chem. Phys. **117,** 8095 (2002).
21. E. A. Coronado and G. C. Schatz, J. Chem. Phys. **19,** 3926 (2003).

22. D. K. Lambert, J. Chem. Phys. **94,** 6237 (1991).
23. M. Sinther, A. Pucci, A. Otto, A. Priebe, S. Diez, and G. Fahsold, Phys. Status Solidi A **188,** 1471 (2001).
24. D. C. Langreth, Phys. Rev. Lett. **54,** 126 (1985).
25. K. Kneipp, Y. Wang, H. Kneipp, L. T. Perelman, I. Itzkan, R. Dasari, and M. S. Feld, Phys. Rev. Lett. **78,** 1667 (1997).
26. S. Nie and S. R. Emory, Science (Washington, D.C.) **275,** 1102 (1997).
27. Z. Zhang and T. Imae, J. Colloid Interface Sci. **233,** 107 (2001).
28. M. Osawa, in *Handbook of Vibrational Spectroscopy*, J. M. Chalmers and P. R. Griffiths, Eds. (John Wiley and Sons, New York, 2002), p. 785.
29. H. D. Wanzenboeck, B. Mizaikoff, N. Weissenbacher, and R. Kellner, Fresenius' J. Anal. Chem. **362,** 15 (1998).
30. N. Al-Rawashdeh and C. A. Foss, Jr., Nanostructured Materials **9,** 383 (1997).
31. S. Y. Kang, I. C. Jeon, and K. Kim, Appl. Spectrosc. **52,** 278 (1998).
32. A. A. Kamnev, L. A. Dykman, P. A. Tarantilis, and M. G. Polissiou, Biosci. Rep. **22,** 541 (2002).
33. C. Domingo, J. V. García-Ramos, S. Sánchez-Cortes, and J. A. Aznárez, ''SERS and SEIR Joint Studies on Gold, Silver and Copper Nanostructures'', in *Proceedings of the XVIII ICORS* (John Wiley and Sons, New York, 2002), p. 295.
34. K. C. Grabar, R. G. Freeman, M. B. Hommer, and M. J. Natan, Anal. Chem. **67,** 735 (1995).
35. E. Garcia-Caurel, E. Bertran, and A. Canillas, Thin Solid Films **398–399,** 99 (2001).
36. Y. Zhu, H. Uchida, and M. Watanabe, Langmuir **15,** 8757 (1999).
37. H. Miyake, S. Ye, and M. Osawa, Electrochem. Commun. **4,** 973 (2002).
38. J. Yang and S.-H. Chen, Appl. Spectrosc. **55,** 399 (2001).
39. A. Rodes, J. M. Orts, J. M. Perez, J. M. Feliu, and A. Aldaz, Electrochem. Commun. **5,** 56 (2003).
40. A. Miki, S. Ye, and M. Osawa, Chem. Commun., 1500 (2002).
41. H. Miyake, S. Ye, and M. Osawa, 204th Meeting, The Electrochemical Society, Orlando, Florida, 2003, p. Abstract 15.
42. N. Goutev and M. Futamata, Appl. Spectrosc. **57,** 506 (2003).
43. J. A. Seelenbinder and C. W. Brown, Appl. Spectrosc. **56,** 295 (2002).
44. J. A. Seelenbinder, C. W. Brown, and D. W. Urish, Appl. Spectrosc. **54,** 366 (2000).
45. C. Domingo, J. V. García-Ramos, S. Sánchez-Cortés, and J. A. Aznarez, J. Mol. Struct. **661–662,** 419 (2003).
46. G. T. Merklin and P. R. Griffiths, Langmuir **13,** 6159 (1997).
47. T. Yoshidome and S. Kamata, Anal. Sci. **13,** 351 (1997).
48. A. Priebe, G. Fahsold, and A. Pucci, Surf. Sci. **482–485,** 90 (2001).
49. Y. Nakao and H. Yamada, Surf. Sci. **176,** 578 (1986).
50. G.-Q. Lu, S.-G. Sun, L.-R. Cai, S.-P. Chen, Z.-W. Tian, and K.-K. Shiu, Langmuir **16,** 778 (2000).
51. S. Zou, R. Gomez, and M. J. Weaver, Langmuir **13,** 6713 (1997).
52. M. Watanabe, Y. Zhu, and H. Uchida, J. Phys. Chem. B **104,** 1762 (2000).
53. A. E. Bjerke and P. R. Griffiths, Appl. Spectrosc. **56,** 1275 (2002).
54. S.-G. Sun, in *Catalysis and Electrocatalysis at Nanoparticle Surfaces*, C. Vayenas, Ed. (Marcel Dekker, New York, 2003), p. 785.
55. A. Priebe, M. Sinther, G. Fahsold, and A. Pucci, J. Chem. Phys. **119,** 4887 (2003).
56. W. H. Yang, G. C. Schatz, and R. P. Van Duyne, J. Chem. Phys. **103,** 869 (1995).
57. P. W. Barber, R. K. Chang, and H. Massoudi, Phys. Rev. B **27,** 7251 (1983).
58. G. C. Schatz and R. P. Van Duyne, in *Handbook of Vibrational Spectroscopy*, J. M. Chalmers and P. R. Griffiths, Eds. (John Wiley and Sons, New York, 2002), p. 759.
59. J. I. Gersten and A. Nitzan, J. Chem. Phys. **73,** 302 (1980).
60. R. K. Chang and T. E. Furtak, *Surface Enhanced Raman Scattering* (Plenum Press, New York, 1982).
61. E. J. Zeman and G. C. Schatz, J. Phys. Chem. **91,** 634 (1987).
62. E. D. Palik, Ed., *Handbook of Optical Constants of Solids* (Academic Press, New York, 1985).
63. R. Hillenbrand, T. Taubner, and F. Keilmann, Nature (London) **418,** 159 (2002).
64. M. Osawa, K.-I. Ataka, K. Yoshii, and Y. Nishikawa, Appl. Spectrosc. **47,** (1993).
65. C. G. Granqvist and O. Hunderi, Phys. Rev. B **16,** 3513 (1977).
66. G. C. Papavassiliou, Prog. Solid State Chem. **12,** 185 (1979).
67. S. Normann, T. Andersson, C. G. Granqvist, and O. Hunderi, Phys. Rev. B **18,** 674 (1978).
68. C. F. Bohren and D. R. Huffman, *Absorption and Scattering of Light by Small Particles* (John Wiley and Sons, New York, 1983).
69. M. Osawa and M. Ikeda, J. Phys. Chem. **95,** 9914 (1991).
70. D. J. Bergman and D. Stroud, Solid State Phys. **46,** 147 (1992).
71. H. J. Fujiwara, P. I. Rovira, and R. W. Collins, Phys. Rev. B **61,** 10832 (2000).
72. E. C. Stoner, Philos. Mag. **36,** 803 (1945).
73. D. J. Jackson, *Classical Electrodynamics* (John Wiley and Sons, New York, 1975).
74. S. Yoshida, T. Yamaguchi, and A. Kimbara, J. Opt. Soc. Am. **61,** 62 (1971).
75. C. F. Eagen, Appl. Opt. **20,** 3035 (1981).
76. R. R. Bilboul, J. Phys. D **2,** 921 (1969).
77. S. Heutz, G. Salvan, S. D. Silaghi, T. S. Jones, and D. R. T. Zahn, J. Phys. Chem. B **107,** 3782 (2003).
78. A. S. Davydov, *Quantum Mechanics* (Pergamon Press, New York, 1965).
79. J. C. Decius and R. M. Hexter, *Molecular Vibrations in Crystals* (McGraw-Hill, New York, 1977).
80. G. Herzberg, *Molecular Spectra and Molecular Structure. II Infrared and Raman Spectra of Polyatomic Molecules* (Van Nostrand, Princeton, NJ, 1945).
81. W. B. Person and G. Zerbi, Eds., *Vibrational Intensities in Infrared and Raman Spectroscopy* (Elsevier Scientific, Amsterdam, 1982).
82. G. Herzberg, *Molecular Spectra and Molecular Structure. III Electronic Spectra and Electronic Structure of Polyatomic Molecules* (Van Nostrand, New York, 1966).
83. R. G. Greenler, J. Chem. Phys. **44,** 310 (1966).
84. H. A. Pearce and N. Sheppard, Surf. Sci. **59,** 205 (1976).
85. R. M. Hexter and M. G. Albrecht, Spectrochim. Acta, Part A **35,** 233 (1979).
86. K. Akers, R. Aroca, A. M. Hor, and R. O. Loutfy, J. Phys. Chem. **91,** 2954 (1987).
87. R. Aroca and S. Rodriguez-Llorente, J. Mol. Struct. **408/409,** 17 (1997).
88. M. J. Frisch, G. W. Trucks, H. B. Schlegel, G. E. Scuseria, M. A. Robb, J. R. Cheeseman, V. G. Zakrzewski, J. J. A. Montgomery, R. E. Stratmann, J. C. Burant, S. Dapprich, J. M. Millam, A. D. Daniels, K. N. Kudin, M. C. Strain, O. Farkas, J. Tomasi, V. Barone, M. Cossi, R. Cammi, B. Mennucci, C. Pomelli, C. Adamo, S. Clifford, J. Ochterski, G. A. Petersson, P. Y. Ayala, Q. Cui, K. Morokuma, D. K. Malick, A. D. Rabuck, K. Raghavachari, J. B. Foresman, J. Cioslowski, J. V. Ortiz, B. B. Stefanov, G. Liu, A. Liashenko, P. Piskorz, I. Komaromi, R. Gomperts, R. L. Martin, D. J. Fox, T. Keith, M. A. Al-Laham, C. Y. Peng, A. Nanayakkara, C. Gonzalez, M. Challacombe, P. M. W. Gill, B. Johnson, W. Chen, M. W. Wong, J. L. Andres, C. Gonzalez, M. Head-Gordon, E. S. Replogle, and J. A. Pople, *Gaussian 98, Revision A.3* (Gaussian, Inc., Pittsburgh, PA, 1998).
89. A. P. Scott and L. Radom, J. Phys. Chem. **100,** 16502 (1996).
90. J.-H. Chang, G. S. Xuan, C. J. Li, and J.-H. Kim, Abstracts of Papers, 223rd ACS National Meeting, Orlando, Florida, April 7–11, 2002, COLL (2002).
91. J. M. Zhang, D. H. Zhang, and D. Y. Shen, Macromolecules **35,** 5140 (2002).
92. T. Imae, in *Encyclopedia of Surface and Colloid Science*, M. Dekker, Ed. (Basel, New York, 2002), p. 3547.
93. A. Ulman, *Ultrathin Organic Films* (Academic Press, Boston, 1991).
94. Z. Zhang, N. Yoshida, T. Imae, Q. Xue, M. Bai, J. Jiang, and Z. Liu, J. Colloid Interface Sci. **243,** 382 (2001).
95. Z. Zhang, T. Imae, H. Sato, A. Watanabe, and Y. Ozaki, Langmuir **17,** 4564 (2001).

96. C. R. Olave, E. A. F. Carrasco, M. Campos-Vallette, M. S. Saavedra, G. F. Diaz, R. E. Clavijo, W. Figueroa, J. V. Garcia-Ramos, S. Sanchez-Cortes, C. Domingo, J. Costamagna, and A. Rios, Vib. Spectrosc. **28,** 287 (2002).
97. M. Campos-Vallette, M. S. Saavedra, G. F. Diaz, R. E. Clavijo, Y. Martinez, F. Mendizabal, J. Costamagna, J. C. Canales, J. V. Garcia-Ramos, and S. Sanchez-Cortes, Vib. Spectrosc. **27,** 15 (2001).
98. H. Nagaoka and T. Imae, Trans. Mat. Res. Soc. Jpn. **26,** 945 (2001).
99. H. Nagaoka and T. Imae, Int. J. Nonlinear Sci. Num. Sim. **3,** 223 (2002).
100. L.-J. Wan, H. Noda, C. Wang, C.-L. Bai, and M. Osawa, Chem. Phys. Chem. **2,** 617 (2001).
101. T. Wandlowski, K. Ataka, and D. Mayer, Langmuir **18,** 4331 (2002).
102. H. S. Kim, S. J. Lee, N. H. Kim, J. K. Yoon, H. K. Park, and K. Kim, Langmuir **19,** 6701 (2003).
103. R. Nakamura, K. Ueda, and S. Sato, Langmuir **17,** 2298 (2001).
104. R. Nakamura and S. Sato, J. Phys. Chem. B **106,** 5893 (2002).
105. R. Nakamura and S. Sato, Langmuir **18,** 4433 (2002).
106. S. Sato, K. Ueda, Y. Kawasaki, and R. Nakamura, J. Phys. Chem. B **106,** 9054 (2002).
107. D. Ferri, T. Buergi, and A. Baiker, J. Phys. Chem. B **105,** 3187 (2001).
108. M. Osawa, in *Near-Field Optics and Surface Plasmon Polaritons,* S. Kawata, Ed. (2001), p. 163.
109. M. Osawa, in *Workshop on Theory and Surface Measurements of Fuel Cell Catalysis,* http://www.scs.uiuc.edu/wieckowski/Lyngby/Lyngby.html, Magleås Conference Center, Høsterkøb, Denmark, 2003.
110. H. Noda, L.-J. Wan, and M. Osawa, Phys. Chem. Chem. Phys. **3,** 3336 (2001).
111. Y. X. Chen, A. Miki, S. Ye, H. Sakai, and M. Osawa, J. Am. Chem. Soc. **125,** 3680 (2003).
112. A. Miki, S. Ye, and M. Osawa, 204th Meeting, The Electrochemical Society, Orlando, Florida, 2003, Abstract 1431 (2003).
113. C. E. Foster, B. P. Barham, and P. J. Reid, J. Chem. Phys. **114,** 8492 (2001).
114. E. Sudo, Y. Esaki, and M. Sugiura, Bunseki Kagaku **50,** 703 (2001).
115. P. R. Griffiths, D. Heaps, and A. Bjerke, Bomem-Michelson Award Symposium, Pittcon 2003, Orlando, Florida (2003).
116. S. Sanchez-Cortes, C. Domingo, J. V. Garcia-Ramos, and J. A. Aznarez, Langmuir **17,** 1157 (2001).
117. A. G. Rand, J. Ye, C. W. Brown, and S. V. Letcher, Food Technol. **56,** 32 (2002).
118. H. Y. N. Holman, D. L. Perry, and J. C. Hunter-Cevera, J. Microbiol. Methods **34,** 59 (1998).
119. R. Aroca and R. Bujalski, Vib. Spectrosc. **19,** 11 (1999).
120. K. Ataka and M. Osawa, J. Electroanal. Chem. **460,** 188 (1999).
121. S. Pronkin and T. Wandlowski, J. Electroanal. Chem. **550–551,** 131 (2003).
122. G. I. Dovbeshko, V. I. Chegel, N. Y. Gridina, O. P. Repnytska, Y. M. Shirshov, V. P. Tryndiak, I. M. Todor, and G. I. Solyanik, Biopolymers **67,** 470 (2002).
123. G. I. Dovbeshko, V. I. Chegel, N. Y. Gridina, O. P. Repnytska, Y. M. Shirshov, V. P. Tryndiak, I. M. Todor, and S. A. Zynio, Semicond. Phys., Quant. Electron. Optoelectron. **4,** 202 (2001).
124. V. F. Chekhun, G. I. Solyanik, G. I. Kulik, V. P. Tryndiak, I. N. Todor, G. I. Dovbeshko, and O. P. Repnytska, J. Exp. Clin. Cancer Res. **21,** 599 (2002).
125. G. I. Dovbeshko, O. P. Repnytska, E. D. Obraztsova, Y. V. Shtogun, and E. O. Andreev, Semicond. Phys., Quantum Electron. Optoelectron. **6,** 105 (2003).
126. W. B. Fischer, G. Steiner, C. Kuhne, and R. Salzer, J. Mol. Struct. **470,** 153 (2001).
127. K. Ataka and J. Heberle, J. Am. Chem. Soc. **125,** 4986 (2003).
128. S. Geng, J. Friedrich, J. Gahde, and L. Guo, J. Appl. Polym. Sci. **71,** 1231 (1999).
129. M. Suzuki, M. Yamamoto, A. Fujishima, T. Miyazaki, H. Hisamitsu, K. Kojima, and Y. Kadoma, J. Biomed. Mat. Res. **62,** 37 (2002).
130. G. V. Andrievsky, V. K. Klochkov, A. B. Bordyuh, and G. I. Dovbeshko, Chem. Phys. Lett. **364,** 8 (2002).